Biomaterials Science

ROYAL SOCIETY OF CHEMISTRY

PAPER

View Article Online
View Journal | View Issue

Cite this: *Biomater. Sci.*, 2022, **10**, 5208

Insulin therapy maintains the performance of PVA-coated PCL grafts in a diabetic rat model†

Yuta Kikuchi, [a] Kyohei Oyama, *[a] Takumi Yoshida,[b] Daisuke Naruse,[c] Masahiro Tsutsui, [a] Shingo Kunioka,[a] Naohiro Wakabayashi[a] and Hiroyuki Kamiya[a]

Vascular tissue engineering has shown promising results in "healthy" animal models. However, studies on the efficacy of artificial grafts under "pathological conditions" are limited. Therefore, in this study, we aimed to characterize the performance of polyvinyl alcohol (PVA)-coated poly-ε-caprolactone (PCL) grafts (PVA-PCL grafts) under diabetic conditions. To this end, PCL grafts were produced *via* electrospinning and coated with the hydrophilic PVA polymer, while a diabetic rat model (DM) was established *via* streptozotocin injection. Thereafter, the performance of the graft in the infrarenal abdominal aorta of the rats was evaluated *in vivo*. Thus, we observed that the healthy group showed CD31 positive/αSM positive cells in the graft lumen. Further, the patency rate of the PVA-PCL graft was 100% at 2 weeks (n = 7), while all the DM rats (n = 8) showed occluded grafts. However, the treatment of DM rats with neutral protamine Hagedorn insulin (tDM) significantly improved the patency rate (100%; n = 5). Furthermore, the intimal coverage rate corresponding to the tDM group was comparable to that of the healthy group at 2 weeks (tDM *vs.* healthy: 16.1% *vs.* 14.7%, p = 0.931). Therefore, the present study demonstrated that the performance of the PVA-PCL grafts was impaired in DM rats; however, insulin treatment reversed this impairment. These findings highlighted the importance of using a model that more closely resembles the cases that are encountered in clinical practice to achieve a clinically applicable vascular graft with a small diameter.

Received 6th April 2022,
Accepted 18th July 2022

DOI: 10.1039/d2bm00531j

rsc.li/biomaterials-science

Introduction

Autologous vessels, such as the great saphenous veins and other peripheral arteries, are the only clinically approved options for small-diameter surgical revascularization, such as coronary artery bypass grafting (CABG) or distal artery bypass grafting.[1] However, autologous vessels are patient-derived; therefore, their poor quality, length, and availability can limit treatment efficacy. Therefore, various vascular tissue engineering approaches have been employed to create off-the-shelf vascular grafts.[2–4]

Owing to their cost-effectiveness, stability, and rapid supply, synthetic polymers are the most widely studied materials in vascular tissue engineering.[5] In particular, polyε-caprolactone (PCL), which is a biocompatible and degradable polymer, has been studied in this regard, and recently, electrospun PCL nanofibers, combined with other materials, have increasingly gained attention as a suitable material for the production of small-diameter vascular grafts.[5–8] However, the hydrophobic property of PCL can activate platelet aggregation, leading to thrombosis.[9,10] Therefore, to improve PCL hemocompatibility, we previously fabricated a PCL nanofiber graft coated with a hydrophilic polymer, polyvinyl alcohol (PVA-PCL graft)[11] and demonstrated its efficacy in a rat model.[12]

Comorbidities are common in patients who require surgical revascularization, and these patients often receive medical treatments to control these comorbidities. Diabetes mellitus (DM), which is the most prevalent comorbidity in cardiovascular disease,[13] is the primary cause of autologous vessel deterioration, including bypass grafts.[14] Insufficient insulin action and the resulting hyperglycemia underlying DM are responsible for all diabetic pathological states. Therefore, insulin therapy is common for both type 1 and 2 DM, and continuous insulin infusion therapy is often performed after cardiovascular surgery for patients with DM. Further, even though insulin is the hormone that functions to lower blood glucose level, it also acts as a growth factor by activating various signaling pathways to exhibit beneficial effects on vas-

[a]*Department of Cardiac Surgery, Asahikawa Medical University, Asahikawa, Hokkaido, Japan. E-mail: koyama@asahikawa-med.ac.jp; Fax: +81-166-68-2499; Tel: +81-166-68-2494*
[b]*Life Materials Development Section, Human Life Technology Research Institute, Toyama Industrial Technology Research and Development Center, Toyama, Japan*
[c]*Business Development section, Business Development and Quality Control Department, Iaazaj Holdings Co., Ltd, Toyama, Japan*

† Electronic supplementary information (ESI) available. See DOI: https://doi.org/10.1039/d2bm00531j

cular systems.[15] This implies that it plays an important role in the treatment of DM and in controlling the vascular tone. Therefore, understanding how DM and insulin treatment affect the behavior of vascular grafts is crucial for developing synthetic vascular grafts that are feasible for clinical applications.

In this study, we aimed to characterize the effect of DM and its treatment with insulin on PVA-PCL graft performance using a rat model.

Experimental

Graft preparation

The PVA-PCL graft was prepared as previously described.[12] Briefly, a PCL nanofiber sheet was electrospun using a 10% polycaprolactone (PCL, M_w 80 000; Sigma-Aldrich, St Louis, MO, USA) solution dissolved in *N*,*N*-dimethylformamide, and tetrahydrofuran (3 : 7, w : w) under the following spinning conditions: applied voltage, 20 kV; tip collector distance, 20 cm; flow rate, 1.7 mL h^{-1}; and spinning rate, 20 rpm. The resulting sheet was cut (width: 20 mm) and wound around a 1 mm polytetrafluoroethylene (PTFE) axle to form a three-layer sheet. After the PTEF axle was removed, the PCL graft was obtained as a tubular scaffold. Further, a PVA solution containing 33.3% (w/w) ethanol was prepared and slowly added to the PCL graft, after which an empty syringe was used to remove the excess solution remaining on the graft. Finally, the grafts were dried overnight at room temperature (approximately 25 °C).

Establishment of DM and treatment of DM rat model

All the animal experiments conducted in this study were approved by the Institutional Animal Care and Use Committee of Asahikawa Medical University (reference number 20129-2, R3-087-02).

In brief, 8–10-week-old male Wister rats (Charles River, Kanagawa, Japan) were used in this study. This is because the male rats offer an anatomical advantage for graft implantation. Further, they are frequently used in vascular graft implantation studies.[16,17] To induce diabetes, the rats were administered streptozotocin (STZ; at a dose of 65 mg kg^{-1}), which destroys pancreatic β cells, *via* injection at the tail vein. After 1 week, the blood sugar (BS) levels of the rats were measured using LAB Gluco (Bio Medical Science, Tokyo, Japan), and based on the results obtained, rats with BS level >300 mg dL^{-1} were considered as DM model rats (Fig. 2A). Conversely, healthy control rats were administered phosphate-buffered saline (PBS).

Further, the DM rats were treated daily *via* the subcutaneous injection of neutral protamine Hagedorn (NPH) insulin (0–10 U per rat). After 5 to 7 days, DM rats with BS <300 mg dL^{-1} were defined as the treatment DM group (tDM) (Fig. 4A). Conversely, the DM control (cDM) rats were administered PBS. The body weights (BWs) and BS levels of the test animals were further monitored daily throughout the experimental period.

Graft implantation and collection

For graft implantation, 8–10-week-old male Wistar rats (Charles River, Kanagawa, Japan) were anesthetized using 5% isoflurane and maintained under 2–3% isoflurane using a small animal anesthesia machine. Thereafter, the abdominal aorta of the rats was isolated through a midline abdominal incision and the inferior vena cava was stripped off. Subsequently, the infrarenal aorta was clamped under the left renal artery and at the bifurcation of the aorta. The aorta was transected and replaced with a PVA-PCL graft with an inner diameter of 1 mm and a length of approximately 5 mm. This replacement was performed *via* end-to-end anastomosis with running sutures using 10-0 polypropylene. After the procedure, the aorta was unclamped and the abdominal incision was closed. The rats were then provided with standard food and water; no antiplatelet or anticoagulant drugs were administered during the follow-up period.

At the endpoints, the patency of the graft was determined by observing pulsating blood flow from the hemi-resection site of the distal aorta of the graft anastomosis (ESI Video 1†) under general anesthesia using 5% isoflurane. Further, the grafts were washed with PBS and fixed with 4% paraformaldehyde (PFA) *via* injection at the cardiac apex, and then the grafts were harvested.

Histological analysis

The harvested grafts were fixed with 4% PFA overnight and thereafter, washed with PBS. Next, they were cut into two longitudinal halves, including the proximal and distal anastomotic vessels, followed by embedding in an optimal cutting temperature (OCT) compound (Sakura Finetek Japan, Tokyo, Japan) and storage at −80 °C. The frozen samples were then sliced (5 μm) using a cryostat at −20 °C and placed on a glass slide for histological analysis.

Hematoxylin and eosin (HE) staining was performed to evaluate the tissue structure and cell coverage on the graft lumen. In brief, the specimen was washed with PBS for 5 min to remove the OCT compound and thereafter, immersed in hematoxylin solution (FUJIFILM, Tokyo, Japan) for 4 min following a 6 min wash with running water. Next, the specimen was immersed in 1% eosin solution (FUJIFILM, Tokyo, Japan) for 2 min and then washed three times with 70% ethanol. Finally, the resulting specimen was encapsulated with Marinol 750 (Muto Puro Chemical Co., Tokyo, Japan) and examined.

For immunofluorescence (IF) staining, heat-induced epitope retrieval was performed using tris-ethylenediaminetetraacetic acid (EDTA) buffer (containing 10 mM Tris base, 1 mM EDTA, and 0.05% Tween 20; pH 9.0), and the specimens were blocked using 1% bovine serum albumin in PBS before antibody reactions. The primary antibodies, anti-CD31 (1 : 200, #AF3628; R&D Systems Minneapolis, MN, USA) and anti-alpha smooth muscle actin (1 : 250, #56856; Cell Signaling Technology, Danvers, MA, USA), and secondary antibodies, Alexa Fluor 488 conjugated anti-goat IgG and Alexa Fluor 555 conjugated anti-mouse IgG (#A-11055 and #A-31570, respect-

ively; Thermo Fisher Scientific, Waltham, MA, USA) were used in this study. Further, Hoechst 33342 (FUJIFILM, 346-07951, Tokyo, Japan) was used for nuclear staining.

HE and IF images were then captured using an all-in-one fluorescence microscope (BZ-X810, Keyence, Osaka, Japan). The intimal coverage rate (ICR) was measured to evaluate endothelialization. Further, using IF images, the intima-covered length (CD31/αSM positive length) of the graft lumen from both proximal and distal anastomotic sites and graft length was measured using ImageJ software,[34] and ICR was calculated using the following formula:

$$\text{ICR}\ (\%) = (\text{intima-covered length}/\text{graft length}) \times 100.$$

Quantitative PCR (qPCR)

To obtain total RNA from rat abdominal aorta, the collected tissue samples were lysed and pre-cleaned using TRIzol™ Reagent (Thermo Fisher Scientific, Tokyo, Japan) and total RNA was purified using the NucleoSpin® RNA kit (Takara Bio Inc., Shiga, Japan) following the manufacturers' instructions. The total RNA was converted to cDNA using the ReverTra Ace® qPCR RT Master Mix (TOYOBO, Osaka, Japan). Thereafter, cDNA corresponding to 5 ng of the total RNA was used for qPCR using the THUNDERBIRD Next SYBR qPCR Mix system (TOYOBO, Osaka, Japan). The primer sequences used in this study are provided in ESI File 1.† Further, target gene expression and bacteria S16 rRNA content were normalized against the internal control, *Rplp0*, and presented as a relative value against that corresponding to the control sample.

Statistical analysis

All statistical analyses were performed using GraphPad Prism 9 (GraphPad Software, San Diego, CA, USA) and EZR version 1.54.[35] Further, all nominal variables were analyzed using Fisher's exact test, while all non-normally distributed quantitative data were analyzed using the Mann–Whitney *U* test. The results for quantitative data were expressed as the median and interquartile range. Statistical significance was set at $p < 0.05$.

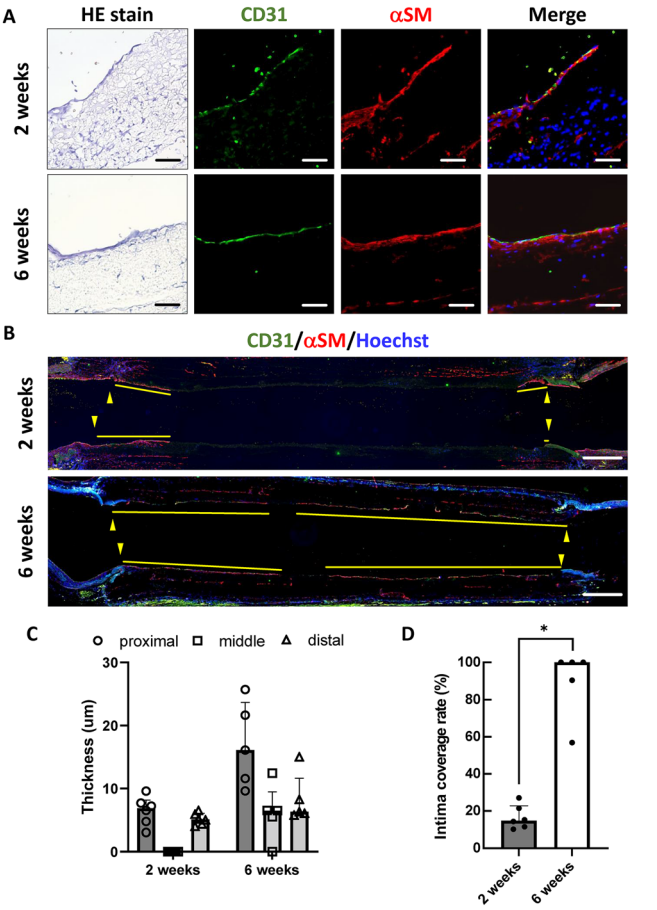

Fig. 1 Performance of the PVA-PCL graft characterized at 2 and 6 weeks after graft implantation in healthy rats. (A) Hematoxylin and eosin (HE) and immunofluorescence (IF) staining results showing endothelialisation. The HE and IF images of the proximal anastomotic site are shown. The endothelial cell marker, CD31 (green) and smooth muscle cell marker, αSM (red) were immunostained. Nuclei were counterstained with Hoechst (blue). Scale bar = 50 μm. (B) Longitudinal images showing intimal coverage. The green arrowheads indicate anastomotic sites, while the green lines indicate the intima-covering range. Scale bar = 500 μm. Quantification of: (C) intimal thickness and (D) intimal coverage rate. The CD31(+)/αSM (+) positive intima thickness at the proximal, middle, and distal sites, and the intima coverage rate were measured. Data are presented as medians, interquartile ranges, and individual values. *$p < 0.05$.

Results

PVA-PCL graft is patent and exhibits endothelialization in healthy rats

To characterize the performance of our previously developed PVA-PCL graft in healthy rats, we implanted the graft into the infrarenal abdominal aorta of the healthy rats under general anesthesia, and after 2 and 6 weeks, collected the grafts for analysis. Thus, we observed that the patency rates at 2 and 6 weeks were 100% (7/7 rats) and 62.5% (5/8 rats), respectively. Further, to evaluate the cellularization of the grafts, HE and IF staining were performed on patent cases (6 rats at week 2 and 5 rats at week 6; one sample failed during the staining preparation at week 2). Thus, the HE images of the proximal anastomotic sites showed autologous cellular engraftment and the formation of thin cell layers on the luminal surface at both 2 and 6 weeks (Fig. 1A). Further, the IF images demonstrated that the cell layers on the luminal surface were positive for CD31 and αSM (α-smooth muscle), confirming intima formation with endothelial and smooth muscle cells. We also observed that the neointima at 6 weeks tended to be thicker than that at 2 weeks (Fig. 1C). Longitudinal images with low magnification showed that endothelialization elongated continuously from both the proximal and distal anastomotic sites at both 2 and 6 weeks; however, no neointimal layer was observed in the middle of the graft at 2 weeks (Fig. 1B). Furthermore, based on the calculation of the ICR, we observed that endothelialization (Fig. 1D) was significantly higher at week 6 than at week 2 ($p = 0.0043$; 100% IQR: 90.4–100, $n = 5$

vs. 14.7% IQR: 12.2–19.9, n = 6 rats). These results demonstrated that the PVA-PCL graft showed patency at 2 to 6 weeks, with endothelialization progressing over time.

Performance of the PVA-PCL graft in DM rats

Patients with DM frequently undergo small vascular revascularization. Therefore, we chose DM as a pathological model and examined its effects on the performance of the PVA-PCL graft. Specifically, we established a DM rat model *via* the administration of STZ, which damages pancreatic β-cells. BS levels were measured after 1 week, and rats with BS levels ≥300 mg dL^{-1} were considered as DM rats. The PVA-PCL graft was then implanted, and the BWs and BS levels of the test animals were recorded daily. PBS was administered to the healthy (control) group (Fig. 2A). Fig. 2B shows the changes in body weights (ΔBWs) of the rats after STZ administration and graft collection at different time points. Notably, the ΔBWs corresponding to the DM group were smaller than those corresponding to the control group (p = 0.1893; 27.5, DM group, n = 8 *vs.* 52, control group, n = 7). This could be due to the absence of insulin secretion.[18] Further, BS levels at graft implantation and harvest were significantly higher for the DM group than the control group (600 *vs.* 180, p = 0.0003 at implantation; and 600 *vs.* 113, p = 0.0003 at harvest; Fig. 2C). To characterize the effect of hyperglycemia on native aorta, qPCR was performed at the time of implantation (1 week after STZ administration). Thus, we observed that nitric oxide synthase (NOS: Nos2 and Nos3) gene expression was significantly downregulated for the DM group (Nos2: 0.19 ± 0.11 fold, Nos3: 0.5 ± 0.22 fold), indicating endothelial dysfunction. The inflammatory cytokine (TNFα, Il6, and IL1β) and NADPH oxidase (Nox1 and Nox2) gene expression levels corresponding to the DM rats were similar to those corresponding to the Control groups (ESI Fig. 1†). However, the DM group showed significantly increased bacteria specific S16 ribosomal RNA (rRNA) content. These findings demonstrated the successful establishment of an STZ-induced DM rat model.

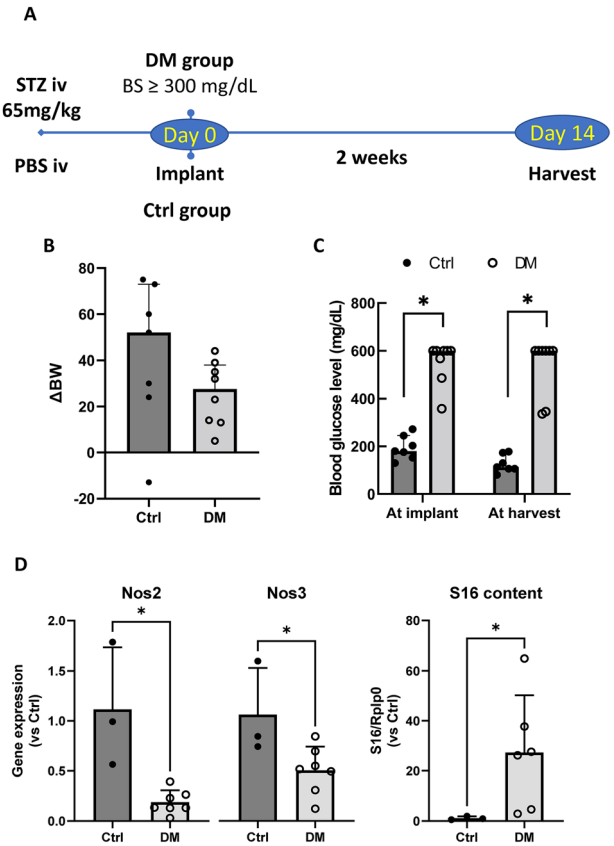

Fig. 2 Establishment of a diabetic rat model (DM). (A) Scheme showing the experimental design. Streptozotocin (STZ; 65 mg kg^{-1}) or PBS (control group) were administered to rats *via* injection at the tail vein. Blood sugar (BS) level was measured 7 days after STZ administration and rats with BS levels ≥300 mg dL^{-1} were defined as the DM group. PVA-PCL grafts were implanted in both groups and harvested 2 weeks after implantation. (B) Body weight changes (ΔBWs) and (C) BS levels at graft implantation and harvest. The ΔBW values indicate changes in BW at a given time point between STZ injection and graft harvest. Data are presented as the median, interquartile range, and individual values. *p < 0.05. BS levels >600 mg dL^{-1} represent pseudo values given that the maximum value the BS tester was able to measure was 600 mg dL^{-1}. Control, Ctrl. (D) Basic characterization of the aorta of STZ-induced DM rats. Abdominal aorta were harvested 7 days after STZ administration, and then gene expression and bacteria specific S16 rRNA contents were measured *via* qPCR. *p < 0.05.

The patency rate observed for the DM group at 2 weeks was significantly lower than that observed for the control group (0%, 0/8 rats *vs.* 74.1%, 5/7 rats; p = 0.007; Fig. 3A). As shown in Fig. 3B, no thrombus was observed in the graft lumen corresponding to the control group. In contrast, 75% and 100% of the grafts in the DM group showed aneurysms and thrombus in the lumen, respectively.

HE staining results (Fig. 3C) showed endothelialization from the anastomotic site in the graft lumen of rats in the control group (Fig. 3C-1a). Conversely, the grafts from the DM rats showed fibrotic tissue adhesion, but not endothelialization (Fig. 3C-2b), indicating thrombotic occlusion (yellow triangle indicates organized thrombus). Additionally, accumulated inflammatory cells (Fig. 3C-2c), such as neutrophils, and bacteria (Fig. 3C-2d) were observed in the graft from DM rats, suggesting an infection. These findings demonstrated that DM negatively impacted the performance of the graft.

Insulin treatment in DM rats improved graft performance

We examined whether therapeutic intervention for DM using insulin could maintain graft performance. Therefore, 7 days after DM induction, the rats were subcutaneously administered NPH insulin once a day, and rats with BS level ≤ 300 mg dL^{-1} after 5–7 days of insulin treatment were defined as the treatment DM (tDM) group (Fig. 4A). Further, rats in the non-treated DM control group (cDM) were administered PBS. Thereafter, the PVA-PCL grafts were implanted in both the tDM and cDM rats and harvested after 2 weeks. During this 2-week period, the BWs and BS levels of the rats were measured daily. Thus, we observed that cDM rats did not show any BW gain, and their BS levels remained high (Fig. 4B and C). Conversely, tDM rats showed significantly increased BWs, and their BS remained below 300 mg dL^{-1} throughout the experimental

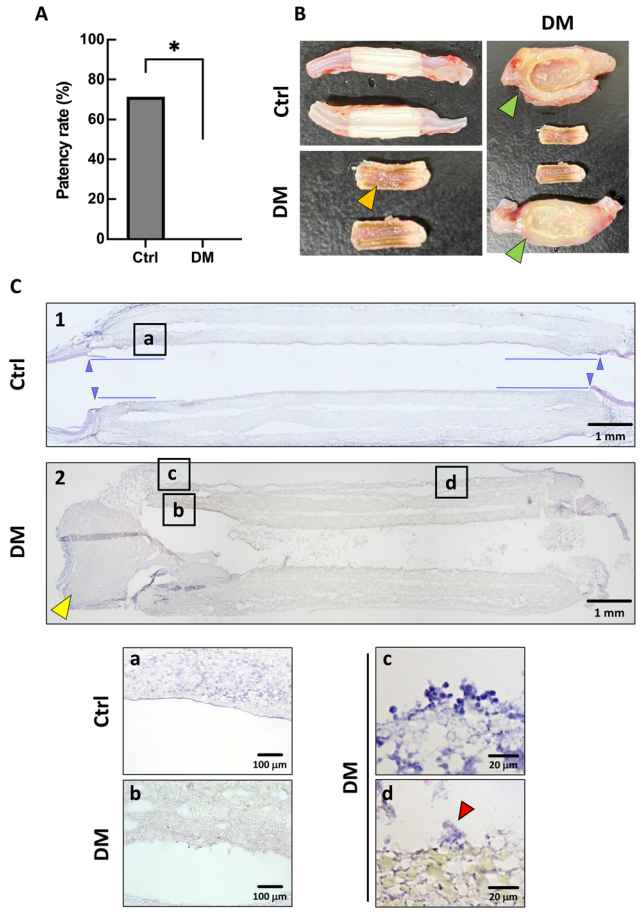

Fig. 3 Effect of diabetes on graft performance. (A) Patency rate. The PVA-PCL graft was harvested 2 weeks after implantation and the patency rate was calculated. *$p < 0.05$. (B) Macro photos of harvested grafts. In DM rats, graft occlusion (orange arrowhead) and aneurysmal formation (green arrowhead) were observed. Representative images are shown (Ctrl, $n = 5$; DM, $n = 5$). (C) Hematoxylin and eosin staining showing: (C1) no thrombus formation and cell coverage at the anastomotic site in grafts from control rats and (C2) thrombus in the graft lumen (yellow arrowhead) in grafts from DM rats. The blue arrow heads indicate anastomotic sites, while the blue lines indicate intima covering range. (a)–(d) in the lower panel represent higher magnification images as indicated in the upper panel. (a) Endothelial layer on the graft lumen in the control group. (b) No neointima formation observed in the DM group. (c) Neutrophils and other inflammatory cells observed in the graft for the DM group. (d) Presence of bacteria in the graft (red arrowhead). DM, diabetic model; Ctrl, control.

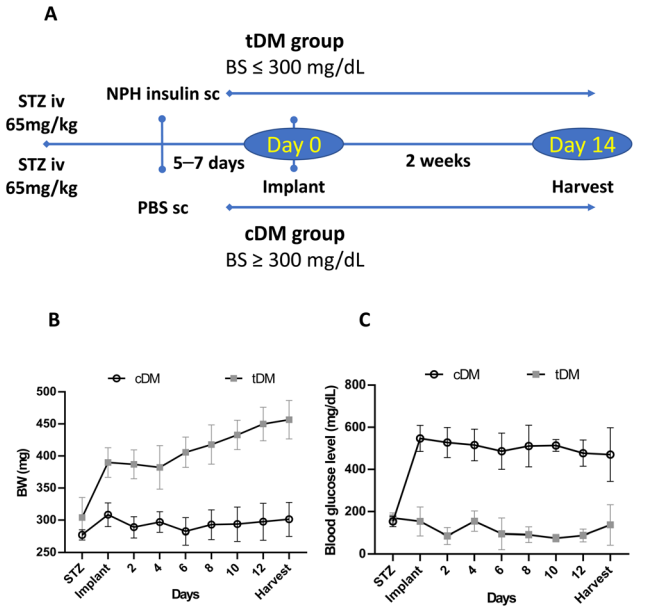

Fig. 4 Establishment of an insulin-treated diabetic rat model (tDM). (A) Scheme of the experimental design. Rats with blood sugar (BS) levels <300 mg dL^{-1} owing to insulin treatment were used as the tDM group. DM was induced *via* STZ administration, and NPH insulin was subcutaneously administered to the tDM group 7 days later. Control diabetic model cDM rats were treated with PBS. After 5–7 days, PVA-PCL grafts were implanted in the cDM and tDM rats. Two weeks after implantation, the grafts were harvested. Body weight (BW) and BS were monitored daily and NPH insulin dose (0–10 U per rat) was adjusted to avoid hyperglycemia and hypoglycemia. (B) BW and (C) BS level monitoring. The tDM rats gained weight compared with the cDM rats. BS level in the tDM group was controlled at <300 mg dL^{-1} and in the cDM group, at >300 mg dL^{-1}.

period, indicating that DM was controlled by insulin treatment (Fig. 4B and C).

Additionally, tDM rats showed significantly higher patency rates than cDM rats (100%, 5/5 rats *vs.* 20%, 1/5 rats; $p = 0.0476$, Fig. 5A). We also observed that the harvested grafts from cDM rats contained thrombi and aneurysms (Fig. 5B), while those from tDM rats showed neither thrombus nor pathological changes (Fig. 5B). In the tDM group, HE staining showed no thrombus formation and cellularization in the graft lumen adjacent to the anastomotic site, which was confirmed to be a neointimal layer *via* CD31/αSM IF staining (Fig. 5C). Further, the ICR corresponding to the tDM group was 16.1% (IQR: 10.5–19.1, $n = 5$; Fig. 5D), which is comparable to that observed for the healthy rats at 2 weeks (14.7%, IQR: 12.2–19.9; $n = 6$). These observations demonstrated that insulin treatment rescued the PVA-PCL graft from DM-induced performance deterioration.

Discussion

Importance of pathological models in evaluating graft performance

The efficacy of tissue-engineered vascular grafts has been predominantly evaluated in healthy animal models;[19,20] however, patients requiring small-caliber surgical revascularization usually have comorbidities. It has also been observed that hyperglycemia increases the risk of vascular occlusion owing to endothelial damage, systemic inflammation, and a hypercoagulability state. Thus, pathological conditions may impact the performance of grafts. In this study, we showed that PVA-PCL grafts were occluded within 2 weeks in DM rats, whereas in healthy rats, the grafts were patent for 6 weeks

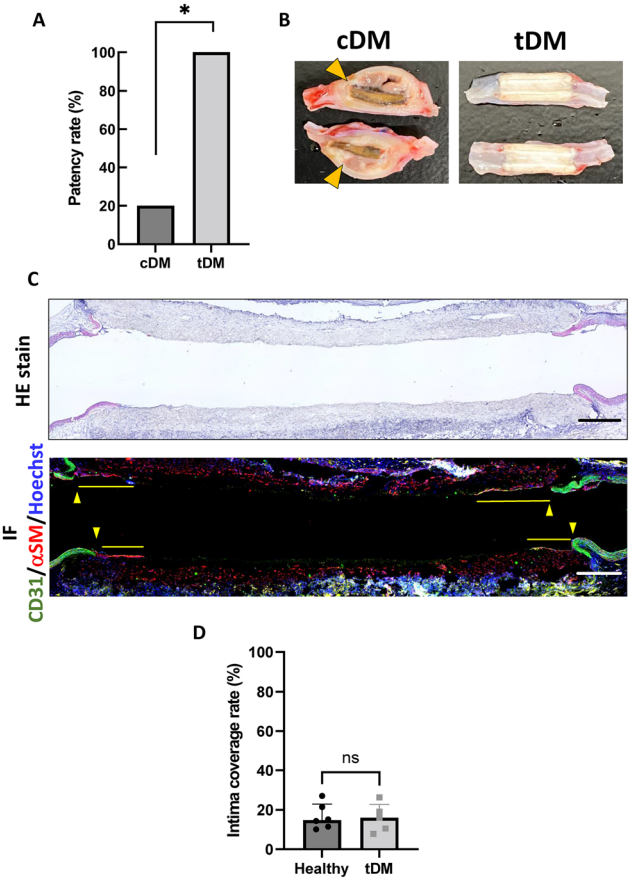

Fig. 5 Effect of insulin treatment on graft performance in the diabetic rat model (DM). (A) Patency rate. PVA-PCL grafts were harvested 2 weeks after implantation and patency rates were calculated. *$p < 0.05$. (B) Macro photos of harvested grafts. cDM rats showed graft occlusion and aneurysmal formation (orange arrowhead). Representative images are shown (control DM, cDM: $n = 5$; treated DM, tDM: $n = 5$). (C) Histological images of grafts in tDM rats. Hematoxylin and eosin and immunofluorescence staining were performed on grafts harvested from rats in the tDM group. In the IF images, CD31 and αSM are shown in green and red, respectively. Nuclei are stained in blue. The green arrow heads indicate anastomotic sites and the green lines indicate intima covering range. Scale bar = 1 mm. (D) Comparison of the intima coverage rates corresponding to tDM and healthy rats 2 weeks after graft implantation.

(Fig. 1 and 3). While various types of small-caliber vascular grafts have been reported, none of them has been applied in clinical practice yet. Perhaps one of the reasons for this is that evaluations of graft function under conditions that reflect clinical practice are limited. Various approaches to promote endothelialization and heparinization, such as the conjugation of bioactive substances, and their promising results have been increasingly reported. Therefore, for future clinical applications, it will be crucial to clarify how these grafts behave in pathologic conditions and study strategies for overcoming these pathologic adverse events that cause systemic vascular occlusions.

Insulin treatment prevents graft deterioration under DM conditions

We demonstrated that insulin treatment in DM prevented the deterioration of PVA-PCL graft performance (Fig. 5). In clinical settings, patients who undergo surgical revascularization often receive treatments to control their comorbidities. Further, clinical studies have suggested that autologous vascular patency is positively correlated with the treatment of comorbidities in small-diameter surgical revascularization. Malmstedt *et al.* reported that patients with well-controlled DM show better bypass graft patency and prognosis after infrainguinal bypass surgery using a prosthetic vascular graft and the saphenous vein than those with uncontrolled DM.[21] Furthermore, using the internal thoracic artery and saphenous vein, Raza *et al.* reported that the presence of DM did not influence the long-term patency of coronary artery bypass grafts when the DM was pharmacologically controlled.[22] Kulik *et al.* also reported that controlling cholesterol levels influences the patency of coronary artery bypass grafts.[23] Thus, comorbidities can lead to the functional failure of bypass grafts even with the use of native vessels. However, controlling such pathologic statuses can improve outcomes. Similarly, our results demonstrated that a synthetic vascular graft could maintain patency under well-controlled pathological conditions using a PVA-PCL graft in an animal model (Fig. 4 and 5). Therefore, we believe that a pathological model with pharmacological intervention simulates clinical conditions. Moreover, evaluating synthetic vascular grafts in such models can increase the feasibility of developing clinically applicable small-caliber vascular grafts.

Mechanisms of PVA-PCL graft deterioration in DM

Our results showed that the patency rate at week 2 after graft implementation was significantly lower in DM rats than in healthy rats (Fig. 3A). Reportedly, the endothelialization of a small-caliber vascular graft is important for preventing graft occlusion in the long term.[24] Additionally, it has been observed that DM causes endothelial dysfunction and delays endothelialization.[25] However, in this study, endothelialization was incomplete at week 2 in healthy rats (Fig. 1C and D), suggesting that the loss of graft function in DM is elicited by endothelialization-independent mechanisms.

An increasing number of reports have shown that hyperglycemia causes hypercoagulability *via* systemic inflammation and endothelial dysfunction of native vessels. In this study, we observed decreased Nos2 and Nos3 expression levels as early as 1 week after STZ administration (Fig. 2D), suggesting that endothelial dysfunction was quickly induced in response to DM. Further, Domingueti *et al.* reported that hyperglycemia increases the production of advanced glycation end product, which increases pro-inflammatory cytokine production in the native vascular endothelium.[14] These pro-inflammatory cytokines can then stimulate the production of pro-coagulant molecules and inhibit the release of anticoagulant factors.[26] Additionally, Kaur *et al.* reported that the glycation of platelet surface proteins can induce platelet hyperactivity.[27] These findings suggest that a

state of systemic hypercoagulability could be induced under hyperglycemic conditions. Moreover, patients with DM are susceptible to infections.[28] In this regard, clinical studies have shown that DM patients with BS levels ≥200 mg dl^{-1}, based on random blood sugar tests, are at a high risk of infection, including surgical site infection.[32,33] Consistent with these findings, the BS levels of the DM rats in this study were much higher than 200 mg dl^{-1} (Fig. 2 and 4) and we further demonstrated that the bacteria-specific S16 rRNA content of DM rat aorta was significantly increased, suggesting an increased infection susceptibility at the time of implantation (Fig. 2D). In addition, bacterial and inflammatory cell accumulation was observed in grafts from DM rats (Fig. 3C-2c and -2d), demonstrating a bacterial infection. An infected arterial wall can be fragile and also result in aneurysmal formation, which could further promote systemic inflammation.[29–31] Therefore, DM could cause a hypercoagulable state *via* infection and systemic inflammation, which hypothetically, are possible factors that contribute to the poor short-term performance of PVA-PCL grafts in DM. The detailed mechanisms still remain to be clarified.

STZ-induced graft deterioration depends on insulin deficiency

We showed PVA-PCL graft deterioration, endothelial dysfunction, and increased infection susceptibility in rats with STZ-induced DM (Fig. 2 and 3). Even though STZ is a well characterized reagent for establishing animal models of DM owing to its ability to damage pancreatic β-cells, some reports suggest that it exerts potential toxicity on off-target tissues and cell types, such as fibroblast and neuroendocrine cells.[36,37] In this study, insulin treatment almost fully rescued graft deterioration induced by STZ treatment accompanied by controlled BS levels (Fig. 4 and 5), suggesting that the observed graft deterioration was dependent on the lack of insulin. This finding is supported by previous reports, which showed that vascular dysfunction in STZ-induced experimental diabetes strictly depends on insulin deficiency.[16,38,39] Taken together, it can be suggested that the PVA-PCL graft deterioration observed in our study is most likely due to an STZ-induced DM pathologic state other than the artifact effect from STZ treatment.

Limitations

In this study, we demonstrated the impact of DM and insulin treatment on PVA-PCL graft performance. However, the study had some limitations. (1) In this study, we did not clarify the mechanism underlying how DM negatively impacted PVA-PCL graft performance. (2) We employed an STZ-induced DM rat model presenting type 1 DM and our data mainly demonstrated the specific effect of hyperglycemia and insulin treatment on PVA-PCL graft performance. However, most patients with DM in clinical practice present with type 2 DM, with much more complex pathological backgrounds. Therefore, to develop clinically applicable synthetic vascular grafts, it will be important to clarify the detailed mechanisms underlying how pathological conditions deteriorate synthetic vascular grafts and conduct further studies using various disease models, including type 2 DM.

Conclusions

In this study, we evaluated the performance of a PVA-PCL graft with a diameter of 1 mm in a DM rat model. Thus, we demonstrated that DM disrupted the function of the PVA-PCL graft and that NPH insulin treatment rescued this deterioration. Various kinds of nanofiber grafts have been developed and their performances have been tested in healthy animal models. Our results indicated that the performance of these nanofiber grafts can be altered in disease conditions. Therefore, it is important to clarify the mechanisms underlying how disease conditions change nanofiber vascular graft performance and develop strategies for overcoming these challenges. Thus, our study highlighted the importance of using a model that more closely reflects the cases that are encountered in clinical practice, taking into consideration patients with comorbidities and the related treatments, to the end of developing clinically applicable small-diameter vascular grafts.

Author contributions

YK performed data collection, analysis, and manuscript writing. MT and SK helped YK with data collection. KO performed data analysis, manuscript writing, and coordination of the study. TY and DN performed material preparation. NW established the methodology of graft implantation into a rat. HK conceived of the study and reviewed the manuscript. All authors read and approved the final manuscript.

Conflicts of interest

There are no conflicts to declare.

Acknowledgements

This research was supported by JSPS KAKENHI Grant Numbers JP21K08812 to Y. K., JP20KK0200 to K. O., JP21K20938 to M. T., and JP19K09258 to H. K.

Notes and references

1 M. F. L. Gaudino, C. Spadaccio and D. P. Taggart, *Interv. Cardiol. Clin.*, 2019, **8**, 173–198.
2 P. Wang, Y. Sun, X. Shi, H. Shen, H. Ning and H. Liu, *Bio-Des. Manuf.*, 2021, **4**, 344–378.
3 Y. Nakayama, M. Furukoshi, T. Terazawa and R. Iwai, *Biomaterials*, 2018, **185**, 232–239.
4 B. B. J. Leal, N. Wakabayashi, K. Oyama, H. Kamiya, D. I. Braghirolli and P. Pranke, *Front. Cardiovasc. Med.*, 2021, **7**, 1–18.
5 H. Rashidi, J. Yang and K. M. Shakesheff, *Biomater. Sci.*, 2014, **2**, 1318–1331.

6 S. de Valence, J. C. Tille, D. Mugnai, W. Mrowczynski, R. Gurny, M. Möller and B. H. Walpoth, *Biomaterials*, 2012, **33**, 38–47.
7 K. Wang, W. Zheng, Y. Pan, S. Ma, Y. Guan, R. Liu, M. Zhu, X. Zhou, J. Zhang, Q. Zhao, Y. Zhu, L. Wang and D. Kong, *Macromol. Biosci.*, 2016, **16**, 608–918.
8 L. Bai, J. Zhao, Q. Li, J. Guo, X. Ren, S. Xia, W. Zhang and Y. Feng, *Macromol. Biosci.*, 2019, **19**, 1–12.
9 I. H. Jaffer, J. C. Fredenburgh, J. Hirsh and J. I. Weitz, *J. Thromb. Haemostasis*, 2015, **13**, S72–S81.
10 V. Leszczak and K. C. Popat, *Appl. Mater. Interfaces*, 2014, **6**, 15913.
11 M. F. A. Cutiongco, D. E. J. Anderson, M. T. Hinds and E. K. F. Yim, *Acta Biomater.*, 2015, **25**, 97.
12 Frontiers in Cardiovascular Medicine (Manuscript ID 946899, under review).
13 B. M. Leon and T. M. Maddox, *World J. Diabetes*, 2015, **6**, 1246–1258.
14 C. P. Domingueti, L. M. Dusse, M. D. Carvalho, L. P. de Sousa, K. B. Gomes and A. P. Fernandes, *J. Diabetes Its Complications*, 2016, **30**, 738–745.
15 M. C. Vázquez and L. Sobrevia, *Curr. Vasc. Pharmacol.*, 2019, **17**, 429–431.
16 M. Oelze, M. Knorr, S. Schuhmacher, T. Heeren, C. Otto, E. Schulz, K. Reifenberg, P. Wenzel, T. Münzel and A. Daiber, *J. Vasc. Res.*, 2011, **48**, 275–284.
17 Z. Wang, W. Zheng, Y. Wu, J. Wang, X. Zhang, K. Wang, Q. Zhao, D. Kong, T. Ke and C. Li, *Biomater. Sci.*, 2016, **4**, 1485–1492.
18 L. H. Baumgard, G. J. Hausman and M. V. Sanz Fernandez, *Domest. Anim. Endocrinol.*, 2016, **54**, 76–84.
19 K. Wang, W. Zheng, Y. Pan, S. Ma, Y. Guan, R. Liu, M. Zhu, X. Zhou, J. Zhang, Q. Zhao, Y. Zhu, L. Wang and D. Kong, *Macromol. Biosci.*, 2016, **16**, 608–618.
20 S. de Valence, J. C. Tille, D. Mugnai, W. Mrowczynski, R. Gurny, M. Möller and B. H. Walpoth, *Biomaterials*, 2012, **33**, 38–47.
21 J. Malmstedt, E. Wahlberg, G. Jörneskog and J. Swedenborg, *Br. J. Surg.*, 2006, **93**, 1360–1367.
22 S. Raza, E. H. Blackstone, P. L. Houghtaling, J. Rajeswaran, H. Riaz, F. G. Bakaeen, A. M. Lincoff and J. F. Sabik, *J. Am. Coll. Cardiol.*, 2017, **70**, 515–524.
23 A. Kulik, A. M. Abreu, V. Boronat and M. Ruel, *Contemp. Clin. Trials*, 2017, **59**, 98–104.
24 Y. Zhuang, C. Zhang, M. Cheng, J. Huang, Q. Liu, G. Yuan, K. Lin and H. Yu, *Bioact. Mater.*, 2021, **6**, 1791.
25 Z. Wang, W. Zheng, Y. Wu, J. Wang, X. Zhang, K. Wang, Q. Zhao, D. Kong, T. Ke and C. Li, *Biomater. Sci.*, 2016, **4**, 1485–1492.
26 S. Margetic, *Biochem. Med.*, 2012, **22**, 49.
27 R. Kaur, M. Kaur and J. Singh, *Cardiovasc. Diabetol.*, 2018, **17**, 121.
28 I. M. Carey, J. A. Critchley, S. Dewilde, T. Harris, F. J. Hosking and D. G. Cook, *Diabetes Care*, 2018, **41**, 513–521.
29 D. J. Kusner, E. L. Luebbers, R. J. Nowinski, M. Konieczkowski, C. H. King and J. R. Sedor, *Kidney Int.*, 1991, **39**, 1240–1248.
30 A. Janoff, *Annu. Rev. Med.*, 1985, **36**, 207–216.
31 K. Havemann and M. Gramse, *Adv. Exp. Med.*, 1984, **167**, 1–20.
32 E. T. Martin, K. S. Kaye, C. Knott, H. Nguyen, M. Santarossa, R. Evans, E. Bertran and L. Jaber, *Infect. Control Hosp. Epidemiol.*, 2016, **37**, 88–99.
33 American Diabetes Association, *Clin. Diabetes*, 2022, **40**, 10–38.
34 C. A. Schneider, W. S. Rasband and K. W. Eliceiri, *Nat. Methods*, 2012, **9**, 671.
35 Y. Kanda, *Bone Marrow Transplant.*, 2013, **48**, 452–458.
36 O. Brenna, G. Qvigstad, E. Brenna and H. L. Waldum, *Dig. Dis. Sci.*, 2003, **48**, 906–910.
37 M. S. Capucci, M. E. Hoffmann, A. De Groot and A. T. Natarajan, *Environ. Mol. Mutagen.*, 1995, **26**, 72–78.
38 C. L. Haughton, D. L. Dillehay and L. S. Phillips, *Lab. Anim. Sci.*, 1999, **49**, 639–644.
39 T. Kobayashi and K. Kamata, *Atherosclerosis*, 2001, **155**, 313–320.